

**MICROWAVE AND HARD X-RAY EMISSIONS
DURING THE IMPULSIVE PHASE OF SOLAR FLARES:
NONTHERMAL ELECTRON SPECTRUM AND TIME DELAY**

Gu Ye-ming* and Li Chun-sheng

Department of Astronomy
Nanjing University
Nanjing, Peoples Republic of China

*Present address:
Institute of Electron Physics
Shanghai University of Science and Technology
Shanghai, Peoples Republic of China

Abstract

On the basis of the summing-up and analysis of the observations and theories about the impulsive microwave and hard X-ray bursts, we have investigated the correlations between these two kinds of emissions. It is shown that it is only possible to explain the optically-thin microwave spectrum and its relations with the hard X-ray spectrum by means of the nonthermal source model. A simple nonthermal trap model in the mildly-relativistic case can consistently explain the main characteristics of the spectrum and the relative time delays.

I. Introduction

In recent years, along with the continuous development of space observations, the investigation of solar high-energy phenomena plays a more and more important role in flare physics. The so-called high-energy phenomena include the high-energy particles produced by the flare energy release, and the electromagnetic emissions from these particles. It is believed that a significant part of the flare energy is released in the form of high-energy particles during the impulsive phase. But the properties of these particles are not clearly known. For example, what is their velocity distribution (thermal and nonthermal)? Are they produced by heating or by acceleration, etc.?

Since we can't detect these particles in the flaring region on the surface of the Sun, we can only observe their emission on the ground or in interplanetary space, or the escaped particles from the Sun. The former is the basic way to understand these particles.

The emissions most closely related to these high-energy particles are microwave, ultraviolet, hard X-ray, and γ -ray emissions. One of the fundamental problems for our theorists is to relate the observational quantities of these emissions with the high-energy particles. All these emissions are detected during the impulsive phase, so they are of impulsive characteristic, i.e. they have fast oscillating time profiles.

By analyzing the temporal, spatial, and spectral character of the microwave and hard X-ray bursts, we can get some important information about the high-energy particles and the flare energy-release region. In this paper, we have investigated the spectral correlations between these two kinds of emissions and the time delays and reached some important conclusions.

For convenience, in the following discussion we use "MW" and "HX" to represent "Microwave" and "Hard X-Ray", respectively. The units of all the quantities used in the paper are listed in Table 1.

Table 1. Quantities used in this paper

Symbols	Meaning	Units
L, S, V	linear dimension, projected area and volume of emission source respectively	10^9 cm , 10^{18} cm^2 10^{27} cm^3
F _x	photon flux of HX	photons $\text{cm}^{-2} \text{ s}^{-1} \text{ keV}^{-1}$
F _{μ}	flux density of MW source	S.F.U.
T _b , T _{eff}	brightness and effective temperature of MW source	10^9 K
B	magnetic field in the source	10^2 Gauss
N ₀	electron density of medium	10^{10} cm^{-3}
N	nonthermal electron density	10^9 cm^{-3}
$\xi = N \cdot N_0 \cdot V$	emission measure	10^{46} cm^{-3}
E, ϵ	electron and photon energy	keV
f	MW frequency	10^9 Hz (GHz)
A	index of power-law spectrum	10^7

II. Impulsive Microwave and Hard X-ray Bursts

To show the purpose of this work and to provide a foundation of our discussion, we give a brief review of both observational and theoretical investigations of MW and HX bursts.

1. Morphology and Time-correlation

Both MW and HX bursts have an impulsive character and have similar structures. Their morphologies are varied. The simplest one is a single-spike event. A multi-impulsive burst may have a very complex time profile. But in general we can resolve a multi-impulsive burst into many single-spike bursts, and all these resolved single-spike bursts are of similar character, with durations between a few seconds and tens of seconds. So it is convenient for us to investigate the short duration single-spike bursts and to extend the results to multiimpulsive bursts (including those with quasi-period structures). We do not consider the so-called "fine-structures" (of subsecond time scale) in this paper.

The time-correlation between MW and HX emissions was recognized as early as the HX bursts from the solar flares were first detected. Space observations have shown that MW and HX bursts are not only similar in time structures, but also reach maximum at approximately the same time and have similar time profiles (we will discuss the time-delays in Section IV). These similarities have been taken as evidence for a common source of MW and HX emissions.

Actually such close correlations show that, even if MW and HX emissions do not come from the same population of electrons in a common source, they should be emitted by the high-energy electrons from the same acceleration process.

2. Spectrum

The observed MW spectrum is composed of data at a few fixed frequencies. The statistical analysis for a large amount of events shows that most of MW bursts have a "C-Type" spectrum. A typical "C-Type" spectrum rises at frequencies of > 1 GHz, and reaches a maximum in the range of ~ 5 -15 GHz, then decays toward higher frequencies. The rise and decay before and after the maximum can be approximately described with power-law spectra (Guidice and Castelli, 1975).

There are three spectral forms used to describe HX spectra: single power-law, double power-law and exponential. But the spectrum represented by them may have differences in essence: the power-law spectrum is of "nonthermal" character, and the exponential one is of "thermal" character. Because of low resolution it is difficult to distinguish between the thermal and nonthermal properties for most of the observed

spectra, but generally a single-power-law fit can describe the main characters of the observed spectra. We will use this form in the following discussions.

3. Thermal and Nonthermal Models for MW and HX Emissions

There have been controversies in deciding the thermal or non-thermal origin of the energetic electrons.

In a thermal model, all the electrons in the energy-release region are bulk-heated to temperatures in excess of 10^8 K. They are trapped in a magnetic loop or an arcade of loops and limited by the ion-acoustic turbulent fronts. The thermal bremsstrahlung and gyrosynchrotron emissions from these hot electrons produce the HX and MW bursts, respectively. In a nonthermal model, a relatively small fraction of the electrons in the energy-release region are accelerated to energies of $E > 10$ -100 keV. They are distributed in an approximate power-law spectrum. There are three limiting cases for HX emission: thin-target, thick-target, and magnetic trap model. Because of the low energy efficiency of the thin-target model, we do not consider it in this paper.

4. Possible Discrimination Between Thermal and Nonthermal Models

It is feasible in principle that, there could be a simple criterion to decide which model is more suitable. But we meet difficulties in reality.

Spectra studies of both HX and MW and their modeling have been undertaken to decide the thermal or nonthermal origin of the energetic electrons. But it has been pointed out that, when the inhomogeneities of the source are introduced, regardless of the spectral forms, the spectra, on their own, are not capable of distinguishing the thermal model from the nonthermal model (Brown, 1974 and Emslie, 1983). Because of the uncertainties in both observations and theories, we can not reach definite conclusions from other observational diagnostics of HX emissions, such as the directivity, polarization and the spatial location of the emission source.

Thus, it can be seen that the only possible way to seek the criteria for distinguishing between the models is to investigate the optically-thin MW spectrum and its morphology (since the optically-thin part is not so seriously affected by the inhomogeneities as the optically-thick part) and their relations with the spectrum and morphology of HX emissions.

Table 2. Data for Impulsive Flare Events

No.	Date	Maximum Time (UT)	Importance H α /SX	Position	τ_{HX}	Delay		MW Spectrum			HX Spectrum		References
						Δt_{MX-MW}	Δt_{MW}	f_{μ}	F_{μ}	m	δ	γ	
1	69.3.25	0205.5	SF	McMath 9994	15	10	+	>17	335	(2.5)	/	(3.2)	(a)
2	69.3.30	0230.53	SN	McMath 10014	10	3	+	>17	211	(2.12)	/	3.6	(a)
3	70.6.14	1250.52	1N	McMath 10389	10	-5.9 \pm 2.5	?	>15.4	52	(3.05)	/	(3.0)	(a)
4	72.5.18	1617.35	1B/M4	Sl6E24	60	?	+	9.4	234	1.76	1.0		(b)
5	80.5.8	1937.15	SB/M2	S22W29	50	0.24	+	7	100	0.5	1.65		(c)
6	80.6.29	0234.33	/M3.6	S25W85	200		+	9.4	320	0.84	1.22	4.6	(d)
7	80.11.1	1919.0	1B/M1.2	N17E64	200	6 \pm 3	\approx 0	6.0	145	1.80	2.3		(e)
8	81.4.1	0146.0	2B/X2.3	S43W52	100	10	+	9.4	5200	1.30	1.27	3.2	(f)
9	81.4.4	0502.5	2B/X1.6	S44W85	80	-6	+	9.4	3050	0.8	0.5	2.55	(f)
10	81.8.11	0145.2	2B/M4.4	Sl3W24	100	8	+	17	1730	1.4	2.3	3.70	(f)
11	80.6.7	0312.2	SB/M7.3	N14W70	60	2	+	17	1000	1.7	1.2	3.10	0.38 (f), (g)
12	80.6.27	1617.0	SB/M6	S27W67	200	?	?	/	/	/	/	3.15	0.067 (h)
13	72.8.4	0626.11	3B/X5	N13E08	1000	?	+(u)	19	25000	(u)	0.9	3.1	(i)
14	72.8.7	1521.20	3B/X5	N14W39	1000	?	+(u)	19	27000	1	1.2	3.0	(i)
15	81.10.15	0444.1	1B/M2.0	S21W14	40	\approx 0	\approx 0	9.4	5340	1.3	2.8	4.1	3.4 (f)
Mean 1.47 1.49 3.41													

References: (a) Crannell et al. 1978; (b) Wiehl et al. 1980; (c) Kaufmann et al. 1983; (d) Dulk and Dennis 1982; (e) Tandberg-Hanssen et al. 1984; (f) Hinotori Symposium on Solar Flares 1982; (g) Kane et al. 1983; (h) Bai et al. 1983; (i) Hoyng et al. 1976.

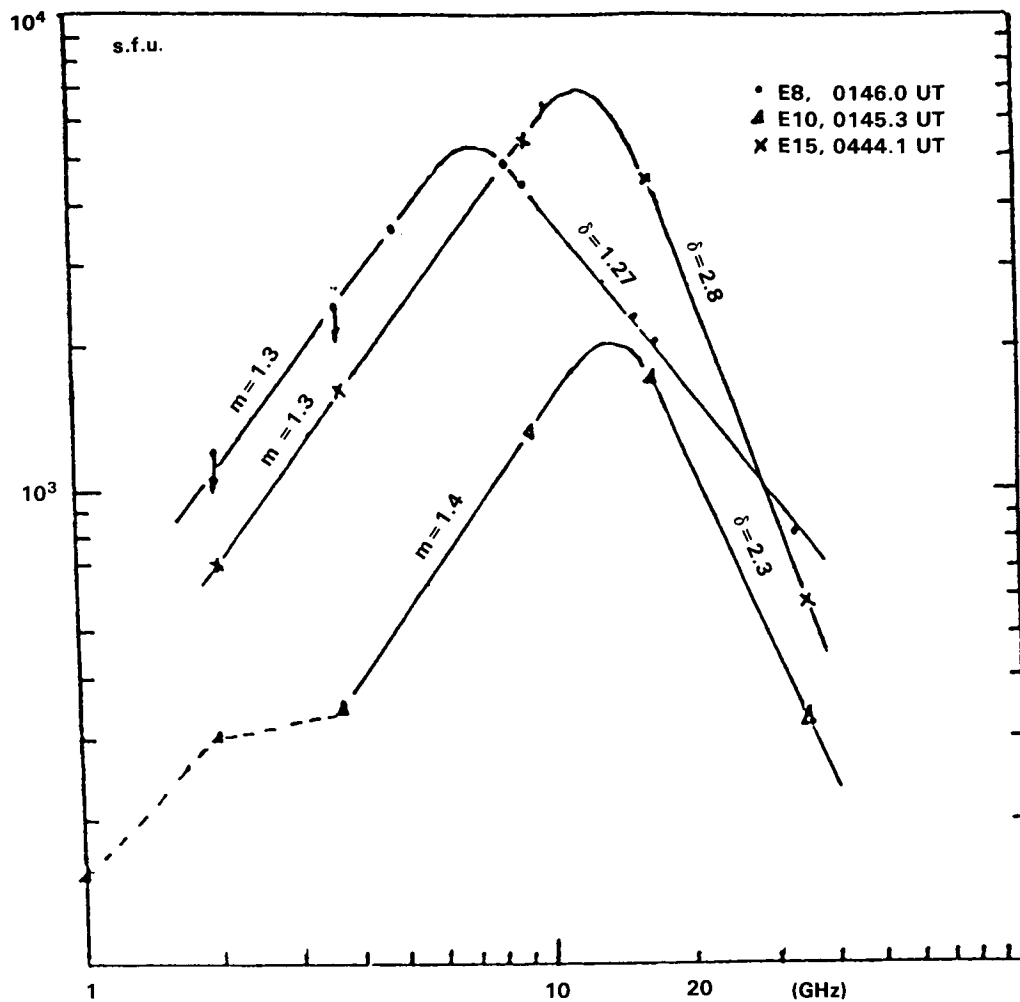


Figure 1. Three typical MW spectra from SGD data.

III. Nonthermal Models of the Emission Source

• Trap Model and Electron-stream Thick-target Model

According to the discussions in the last section, we now try to find criteria to distinguish the two models.

1. Collection of Observational Data

We list the observational data for 15 impulsive events in Table 2. Spectral data for both MW and HX bursts are given for the peak time.

For multi-impulsive (or the so-called "extended bursts") we consider the main impulsive spike. The maximum time is given for the HX burst. Two kinds of delays are given: $\Delta t_{\text{HX-MW}}$ is the delay between HX and MW, a positive value for HX preceding MW; Δt_{MW} is the frequency dependent delay of MW and a positive value is for the precedence of higher frequencies. Most of the MW data are from Solar Geophysical Data (SGD). F_{μ} is the maximum observed flux and f_{μ} is the frequency at which the maximum is reached; m and δ are the power-law indices before and after the maximum (reverse frequency), respectively. All the HX spectral data are selected from the literature. γ is the single power-law index and A is the coefficient of the HX spectrum.

2. Two Nonthermal Models: Model I and Model II

It would be of great significance to explain the main characteristics of MW and HX bursts with a simple model and to make reasonable estimates of the source parameters from the observed data. Crannell et al. (1978) used a homogeneous thermal model to explain 22 simple spike bursts. In this section we will use two kinds of homogeneous nonthermal models instead.

Suppose that, in the energy-release region near the top of the magnetic loop in corona, a fraction of electrons is accelerated to a distribution which can be approximated by

$$N(E) = KE^{-\alpha} \text{ (cm}^{-3}\text{keV}^{-1}\text{)} \quad (1)$$

$$\text{where } K = (\alpha-1)E_0^{\alpha-1}N \quad (2)$$

N is the total number density of the nonthermal electrons with energies $E > E_0$, and E_0 is the low cut-off energy of the power-law spectrum. The accelerated electrons may be trapped in magnetic loops or precipitate along the magnetic lines to the denser solar atmosphere. The energy-spectrum of the freely precipitating electron stream is given by:

$$F(E) = N(E) \sqrt{2/m_e} E^{1/2} S = 1.88 \cdot 10^{27} S K E^{-\alpha+1/2} \text{ (electrons/cm}^2\text{s)} \quad (3)$$

where we have assumed that the magnetic loop has a uniform cross-section with area S . The observed HX spectrum is described as:

$$F_x(\epsilon) = 10^7 A \epsilon^{-\gamma} \quad (4)$$

According to Brown (1974, 1976), the relations between electron spectra and HX photon spectra can be given by:

$$N(E)N_0V = 3.61 \cdot 10^{11} \gamma(\gamma-1)^2 B(\gamma-1/2, 3/2) A E^{-\gamma+1/2} \quad (5)$$

$$F(E) = 2.68 \cdot 10^{40} \gamma^2 (\gamma-1)^2 B(\gamma-1/2, 3/2) A E^{-\gamma-1} \quad (6)$$

for the two cases: trap (Model I) and precipitation (Model II), respectively. $B(p,q)$ is the Beta function. Comparing (1), (5) with (3), (6) we get the relationships between source parameters and observational quantities:

$$\text{Model I: } A = 2.77 \cdot 10^{-3} \xi K_1 \text{ or } \xi = 3.61 \cdot 10^2 A/K_1 \quad (7)$$

$$\text{Model II: } A = 7.01 \cdot 10^2 \text{SN} K_2 \text{ or } \text{SN} = 1.43 \cdot 10^{-3} A/K_2 \quad (8)$$

$$\text{where } K_1 = K/(\gamma(\gamma-1)^2 B(\gamma-1/2, 3/2)); \quad K_2 = K_1/\gamma \quad (9)$$

The corresponding relationships between the spectral indices are

$$\alpha_1 = \gamma - 1/2; \quad \alpha_2 = \gamma + 3/2 \quad (10)$$

To calculate the gyrosynchrotron emission from HX emitting electrons, we use the empirical formulae derived from the numerical method given by Dulk and Dennis (1982). It is convenient to express the peak (spectral reverse) frequency and effective temperature as:

$$f_{\text{peak}} = 35.9 \cdot 10^{-0.21\alpha} (\sin\theta)^{x_4} (NL)^{x_1} B^{x_2} \quad (11)$$

$$T_{\text{eff}} = 4.16 \cdot 10^{-0.26\alpha} (\sin\theta)^{x_5} B^{-x_3} f^{x_3} \quad (12)$$

The emission and absorption coefficients are given by

$$\eta_f = 1.56 \cdot 10^{-12-1.02\alpha} (\sin\theta)^{x_6} B^{d+1} N_f^d \quad (13)$$

$$K_f = 2.67 \cdot 10^{-3.0-0.76\alpha} (\sin\theta)^{x_7} B^{x_5-1} N_f^{x_8} \quad (14)$$

where we use the indices

$$\begin{aligned} x_1 &= 0.32-0.03\alpha; & x_2 &= 0.68+0.03\alpha; & x_3 &= 0.50+0.085\alpha \\ x_4 &= 0.41+0.03\alpha; & x_5 &= -0.36-0.06\alpha; & x_6 &= -0.43+0.65\alpha \\ x_7 &= -0.09+0.72\alpha; & x_8 &= 1.30+0.98\alpha; & d &= 0.90\alpha-1.22 \end{aligned} \quad (15)$$

For a source with brightness temperature T_b , the MW emission flux observed on the Earth is given by

$$F_\mu(f) = S/4\pi R^2 \cdot 2kf^2/C^2 \cdot T_b \quad (\text{in c.g.s. units})$$

where R is the distance between the Earth and the Sun. According to the solution of radiation transfer in a homogeneous source, we have

$$T_b = T_{\text{eff}} (1 - e^{-\tau_f}); \quad \tau_f = 10^9 L K_f \quad (16)$$

$$\text{and } F_\mu(f) = 1.08 S f^2 T_b = 1.08 S f^2 T_{\text{eff}} (1 - e^{-\tau_f}) \quad (17)$$

where τ_f is the optical depth of the source.

It is obvious that the observed spectra of HX and MW emissions are completely determined by the nonthermal electron spectrum (N, E_0, α) and the source parameters (B, L, S, V). For simplicity we take $E_0 = 20$ keV and assume

$$S = L^2, V = SL = L^3 \quad (18)$$

in the following discussion.

3. Evidence for a Nonthermal Electron Spectrum

Correlation between the Indices of the Optically-thin MW and HX Spectra

In a nonthermal source, the optically-thin MW spectrum is determined only by the electron spectrum; it is independent of the inhomogeneities of the source parameters. Its spectral index is the same as that of the emission efficiency given by (13):

$$\delta = d = 0.90\gamma - 1.22 \quad (19)$$

From (10) and (19) we can get the relations between the spectral indices of optically-thin MW and HX emissions for the two models, respectively:

$$\text{Model I: } \delta = 0.90\gamma - 1.67 \quad \text{or} \quad \gamma = 1.11\delta + 1.86 \quad (20.a)$$

$$\text{Model II: } \delta = 0.90\gamma + 0.13 \quad \text{or} \quad \gamma = 1.11\delta - 0.14 \quad (20.b)$$

which are valid for both homogeneous and inhomogeneous sources.

For comparison, let's see the behavior of the optically-thin MW spectrum in the thermal model. For a thermal source with temperatures of $>10^8$ – 10^9 K, both analytical derivation and numerical analysis (Matzler 1978 and Dulk et al., 1979) shows that the optically-thin thermal gyro-synchrotron spectrum produced by the mildly-relativistic thermal electrons is very steep, typically with a spectral index of ~ 7 or 8 . But for a typical HX spectral index of $\gamma = 4$, the corresponding optically-thin MW spectral index is $\delta = 2.38$ and $\delta = 3.74$ for Model I and Model II, respectively. Observations obviously support the nonthermal models. The statistical results of Das and Das Gupta (1983) show that usually the index δ is between ~ 0.5 and 3 and the mean value for 20 events is 1.05 . In Table 2 the mean value of δ is 1.49 for 11 events. It can be seen from the above discussion that no thermal model can explain such hard MW spectra.

We can conclude from (20) that, if both MW and HX emissions are produced by the same population of electrons or by the electrons with the same distribution in energy, there should be a definite relation between the two kinds of emissions. Benz (1977) noticed such a relation.

But instead of (19) he used the highly relativistic approximation

$$\delta = (\alpha - 1)/2 = (\gamma - 3/2)/2$$

(for the trap case) to explain the spectral correlations observed during two outstanding flares. For electrons with energies of >100 keV, the highly relativistic approximation is not suitable.

We plot a δ - γ correlation diagram in Figure 2 by using the data in Table 3. Although the observational data points are relatively few, we can see from Figure 2 that there is a relationship between δ and γ . The following conclusions can be made from Figure 2: (a) Usually the nonthermal models, especially the nonthermal trap model (Model I), can explain the relation between the two kinds of spectral index for most of the impulsive events. (b) It is not excluded that the highly relativistic electrons may make a relative contribution to the high frequency MW spectrum. Some observations of the continuous γ -ray spectrum support such a possibility. (c) MW, especially high frequency MW, emissions mainly come from energetic electrons with energies of $E > 100$ -300 keV.

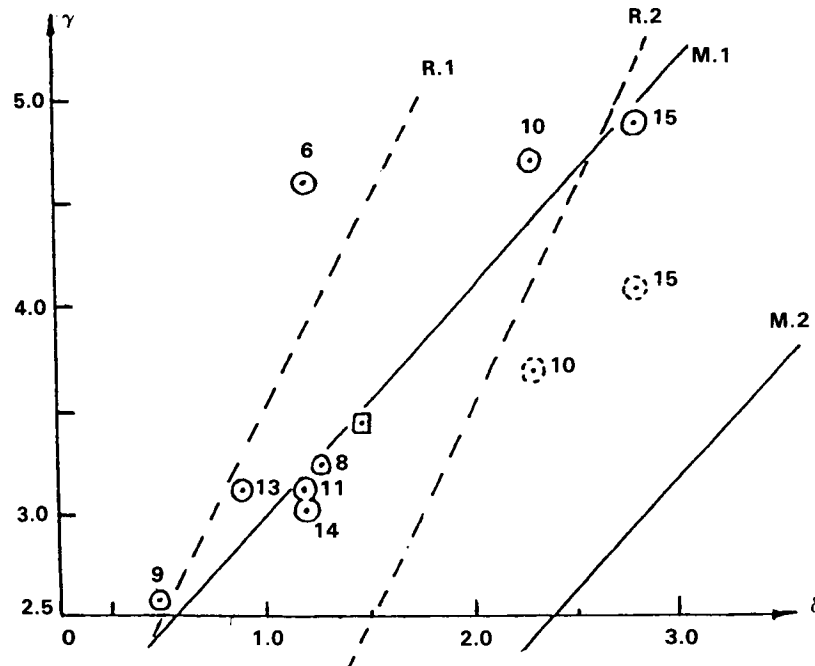


Figure 2: δ - γ correlation diagram. Dotted circles is for the HX spectral indices in the low energy range in double-powerlaw fit events. The small square is for the main values of δ and γ given in Table 2. The lines M.1 and M.2 are the theoretical correlation curves predicted by Model I and II (according to (20)), and R.1 and R.2 are for the high-relativistic approximation: $\delta = (\alpha-1)/2$, α is given by (10).

Table 3

Table 3. Spectral indices of optically-thin MW and HX emissions. $\Delta\epsilon$ is the energy range for observation. The double-power-law fit parameters are given when it is appropriate.

Event No.	MW Spectrum		HX Spectrum			
	f_μ	δ	γ	$\Delta\epsilon(\text{keV})$	γ'	$\Delta\epsilon'(\text{keV})$
6	9.4	1.22	4.6	20-200		
8	9.4	1.27	3.2	20-400		
9	9.4	0.5	2.55	20-350		
10	17	2.3	3.70	20-120	4.71	>120
11	17	1.2	(1.50)	(<69)	3.10	>69
13	19	0.9	3.1	>30		
14	19	1.2	3.0	>30		
15	9.4	2.8	4.1	20-300	4.9	300-600

4. Application of Nonthermal Models to HX and MW Bursts

Now we use Model I and II discussed above to estimate the parameters of flare sources. To relate the observational quantities to source parameters, we extend the optically-thick MW spectrum to $f=f_\mu$ (taking $\tau_f = \infty$ and $f = f_\mu$ in (17)) and write

$$F_\mu = F_\mu(f_\mu) = 4.49 \cdot 10^{-0.26\alpha} (\sin\theta)^{x5} L^2 B^{-x3} f_\mu^m \quad (21)$$

$$\text{where } m = 2 + x3 = 2.5 + 0.085\alpha \quad (22)$$

$$\text{and } f_\mu = f_{\text{peak}} = 35.9 \cdot 10^{-0.21\alpha} (\sin\theta)^{x4} (NL)^{x1} B^{x2} \quad (23)$$

For an event with observed parameters (A, γ) and (f_μ, F_μ) , we can solve the source parameters (N, α) and (B, L) from equations (8) (10) (21) (23) in Model II. In Model I, the emission measure is determined by the HX spectral coefficient A through (7). But since another source parameter N_0 is added in Model I, we introduce a new parameter $H = N/10N_0$, and the source parameters can be solved from equations (7) (10) (21) (23) for any given value of H .

Considering the first order of approximation in our simple models, we take $\theta = 45^\circ$ in the following calculations. The calculated results are given in Table 4 and 5. The results show: (a) Although we used the simplest nonthermal models, we can get good estimates of the burst

Table 4

The observed quantities of the MW and HX spectra and the source parameters calculated in Model I for two H values.

No.	MW Spectrum		HX Spectrum		Source Parameters with H = 0.001				Source Parameters with H = 0.01				ξ
	f_{μ}	F_{μ}	γ	A	B	L	N	N_0	B	L	N	N_0	
1	17	335	(3.2)	(0.003)	10.67	0.87	0.013	1.26	7.27	0.76	0.049	0.49	0.011
2	17	211	3.6	0.097	8.56	0.71	0.055	5.49	5.98	0.62	0.21	2.13	0.11
3	15.4	52	(3.0)	(0.002)	7.20	0.32	0.061	6.06	4.84	0.28	0.24	2.37	0.013
6	12	360	4.6	8.5	7.79	1.90	0.028	2.77	5.79	1.67	0.106	1.06	0.526
7	7.5	6000	3.2	0.07	3.10	7.20	0.0026	0.257	2.11	6.26	0.010	0.10	0.247
8	11	3300	2.55	0.06	2.37	2.48	0.03	3.02	1.55	2.15	0.118	1.18	1.39
10	14	2500	3.70	1.3	6.10	2.88	0.021	2.13	4.29	2.52	0.083	0.83	1.08
11	17	1000	3.10	0.38	4.71	1.09	0.116	11.7	3.19	0.95	0.48	4.56	1.79
15	12	8000	4.1	3.4	7.02	7.49	0.0046	0.46	5.06	6.57	0.18	0.18	0.894
mean					6.42	2.77	0.0037	3.66	4.45	2.42	0.14	1.4	0.67

Table 5

The observed quantities of the MW and HX spectra and the source parameters calculated in Model II.

No.	MW Spectrum		HX Spectrum		Source Parameters			
	f_{μ}	F_{μ}	γ	A	B	L	N	T_b
1	17	335	(3.2)	(0.003)	21.3	2.04	3.66×10^{-4}	0.26
2	17	211	3.6	0.097	14.4	1.52	8.30×10^{-3}	0.29
3	15.4	52	3.0	(0.002)	15.1	0.75	2.76×10^{-3}	0.36
6	12	360	4.6	8.5	12.3	4.12	8.40×10^{-3}	0.14
8	7.5	6000	3.2	0.07	7.76	18.0	1.09×10^{-4}	0.31
9	11	3300	2.55	0.06	5.94	5.72	3.61×10^{-3}	0.77
10	14	2500	3.70	1.3	10.5	6.17	5.35×10^{-3}	0.31
11	17	1000	3.10	0.38	8.28	2.25	4.71×10^{-2}	0.63
15	12	8000	4.1	3.4	12.1	16.6	7.27×10^{-4}	0.19
mean					12.0	6.35	8.52×10^{-3}	0.35

source parameters. (b) Comparing the results in Table 4 and 5, it can be seen that the source parameters derived in the trap model (Model I) are more reasonable than those derived in the precipitation model (Model II), since it seems not possible that the magnetic field in the corona is stronger than 1000 G. This tends to support the trap model and is consistent with the conclusion from the above analyses of spectral correlation. But the strong magnetic fields of 800-2000 G calculated in Model II suggest that, in the freely precipitating thick-target model the position of MW source should be near the foot of the magnetic loop or loops, where the magnetic field is much stronger than that at the top of the loop. (c) Comparing the results for different H values in Table 4, we find that in the magnetic region where the emitting electrons are trapped, the ratio of nonthermal electrons to medium electrons, H , may have very different values for different events.

IV. Time Delays of MW and HX Bursts

Observations with high time resolution have shown that there are delays between the time structures of different kinds of emission. We will give a simple explanation for these delays

1. Characters of Time Delays

Some data about the delays was given in Table 2. It can be seen that, for most of the events HX precedes MW. The time difference is from a few hundreds of milliseconds to tens of seconds. The high frequency MW ususally precedes the low frequency MW and the low energy HX precedes the high energy HX. All these may be taken as the regular pattern of the delays. But there also exist some unusual delay patterns, such as event No. 3 and No. 9 in Table 2.

Morphologically, the time delays can be divided into three kinds; (a) "profile delay", i.e. the time profiles of the two kinds of emission show a systematic shift; (b) "peak delay", i.e. both of the emissions start to rise at nearly the same time but the times for them to reach the maximum are different; (c) "start-time delay", i.e. both of the emissions peak at the same time but with different start times. Different kinds of delays may correspond to different mechanisms in the emission source.

2. Explanation of the Time Delays

Both the frequency-dependent and energy-dependent delays are the manifestations of the temporal evolution of emission spectra (Ref. e.g., Takakura et al. 1983). In a nonthermal model the evolution of the emission spectrum corresponds to that of the electron spectrum. The usual pattern of the spectral evolution of HX emission is "soft-hard-soft" and the spectrum is hardest at the time of peak flux. But some

events show continuous hardening in HX spectrum after the peak flux is reached.

Having carefully investigated the relationship between the spectral evolution and time delays, we find that: if the HX spectrum is hardest at the peak time, there is no time delay longer than a second between HX and MW; for events with long HX to MW delay (longer than a few seconds), the HX spectrum continues to harden after the peak.

According to the above discussions, we know that MW, especially the high frequency MW emissions (in the optically-thin part), are mainly contributed by the electrons with energies of $E > 100-300$ keV. The hardening of the HX spectrum reflects the hardening of electron spectrum. Under certain conditions, there may be a case where the total number of nonthermal electrons (with $E > E_0$) is decreasing but the number of the electrons with higher energies (e.g. with $E > 100$ keV) is increasing. This can cause the peak delay of MW relative to HX and the energy-dependent delay of HX. The continuous hardening of the HX spectrum after the maximum time of the event may correspond to the energy-dependent life time of electrons trapped in the magnetic loop (Enome 1982) or to second-step acceleration during the impulsive phase.

To see the actual relation between time delay and the evolution of electron spectrum, we use Model I to make a quantitative analysis.

We choose event No. 2 for our analysis. In Table 4 we choose the parameter values corresponding to $H = 0.1\%$ for the following calculation. Suppose that the source parameters L , N and B are constants during the lifetime of the event and the acceleration process rises and decays with exponentially according to the following expressions:

$$\begin{aligned} N(t) &= N \cdot \exp((t-t_m)/t_{01}) \text{ for } t \leq t_m \\ &= N \cdot \exp((t_m-t)/t_{02}) \text{ for } t > t_m \end{aligned} \quad (24)$$

where t_m is the maximum (peak) time of the event (when the nonthermal electron number reaches maximum) and t_{01} , t_{02} are the characteristic times for the rising and the decay phase respectively. To simplify the calculation we take $t_m = 2t_{01}$ and assume two cases for the decay phase as illustrated in Figure 4,

$$(a): t_{02} = t_{01} = 4s$$

$$(b): t_{02} = t_{01}/2 = 4s$$

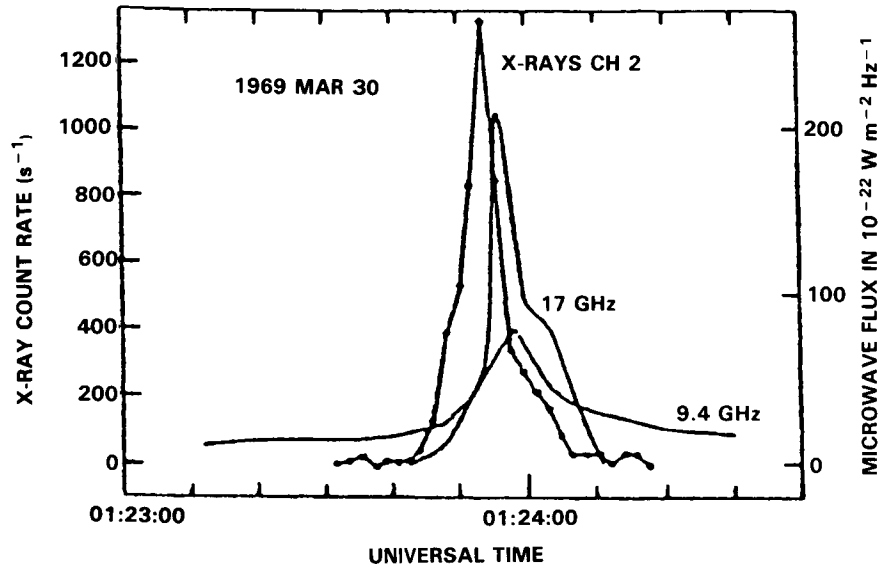


Figure 3. The time profiles of the HX flux in the energy range 28–55 keV and 9.4 and 17 GHz MW flux, copied from the Crannell et al. (1978).

The time evolution of the HX spectral index $\alpha(t)$ is plotted in Figure 4. We also assumed two cases to correspond to that of $N(t)$. In both cases the minimum time of $\alpha(t)$ is delayed from t_m by several seconds but with no softening in case (b). By introducing the time evolution of $N(t)$ and $\alpha(t)$, we can calculate the time profiles of HX and MW emissions. The calculated profiles are illustrated in Figure 5a and 5b corresponding to case (a) and (b) in Figure 4, respectively. The MW flux was calculated for two frequencies of 9.4 and 17 GHz and the HX photon flux is given for a photon energy of $\epsilon = 41.5$ keV, which is the logarithmic middle energy of the second channel of the HX spectrometer on OSO-5 (ref. Crannell et al. 1978).

Thus, it can be seen that the HX to MW delay can be explained very well in the present model (comparing Figure 3 and Figure 5). The longer delay of low frequency MW (e.g. 9.4 GHz) emission is probably caused by the expansion of the optically-thick emission source. The energy-dependent delay of HX can also be explained in this model. It is interesting that the rare "reversed" delay (with MW preceding HX, such as event No. 3 and No. 9) could be easily explained if we reverse the time axes in Figure 4 and Figure 5. The physical meaning of this reverse may be that the second-step acceleration ceases before the maximum time of the event.

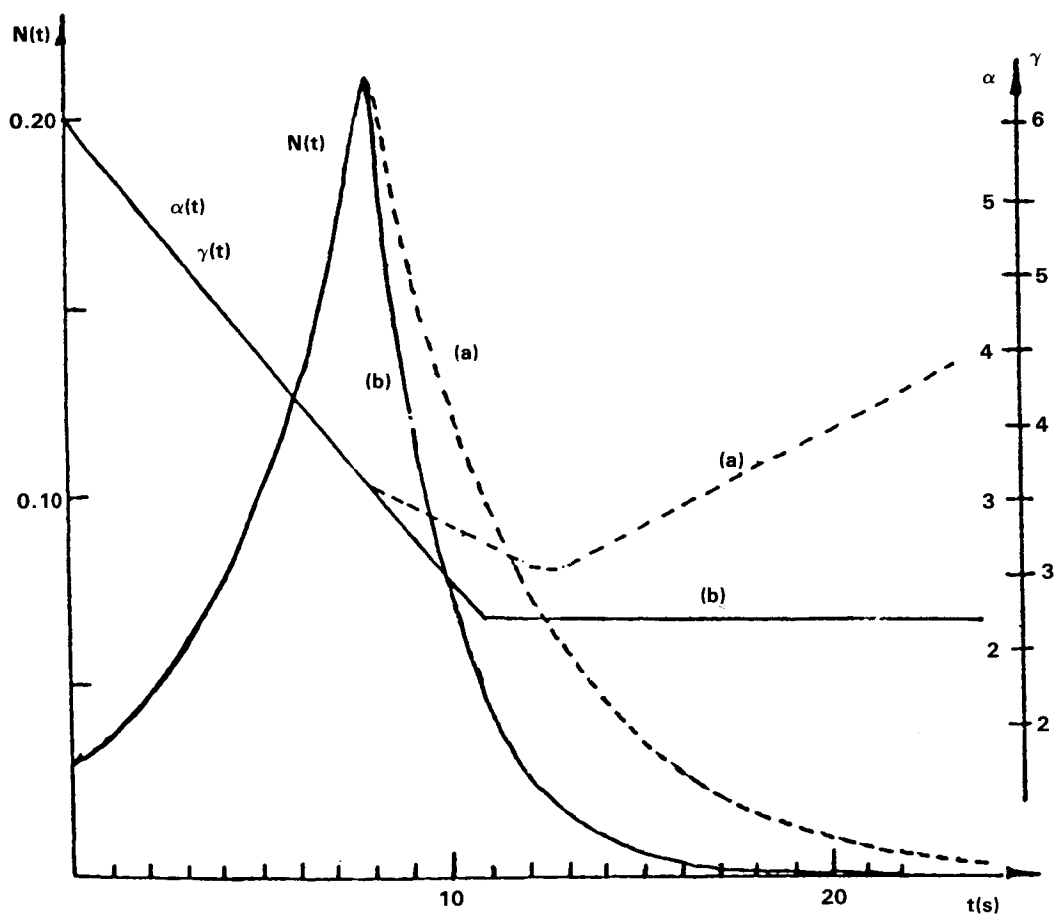


Figure 4. The supposed time evolution of the nonthermal electron spectrum in event No. 2. $N(t)$ is determined by (24) and (25). $\alpha(t)$ (then $\gamma(t)$) is inferred from the data given by Crannell et al. (1978, Figure 12).

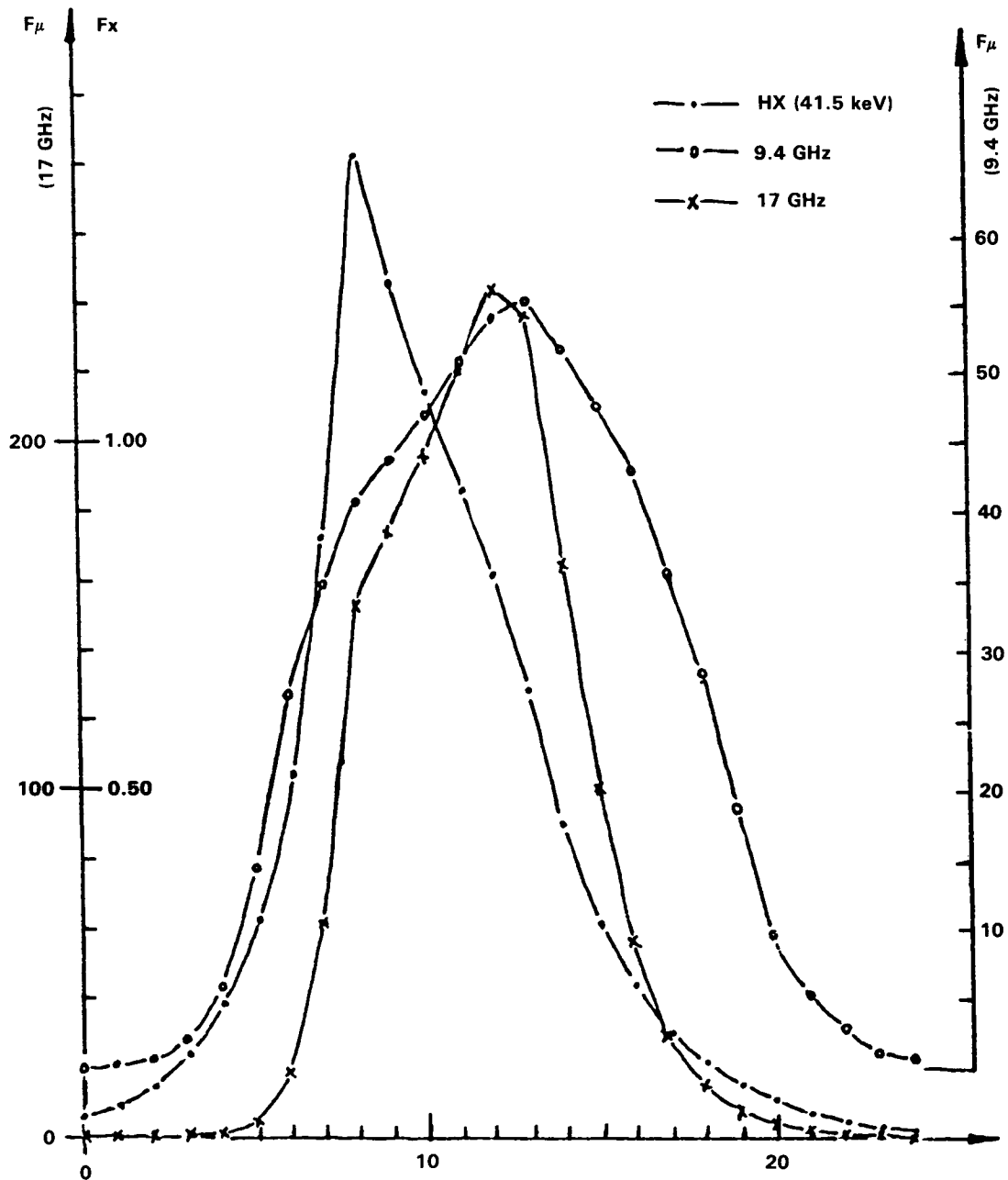


Figure 5a. The calculated time profiles of the HX flux at 41.5 keV and MW flux at 9.4 and 17 GHz, corresponding to case (a) in Figure 4, with a symmetric time profile of $N(t)$.

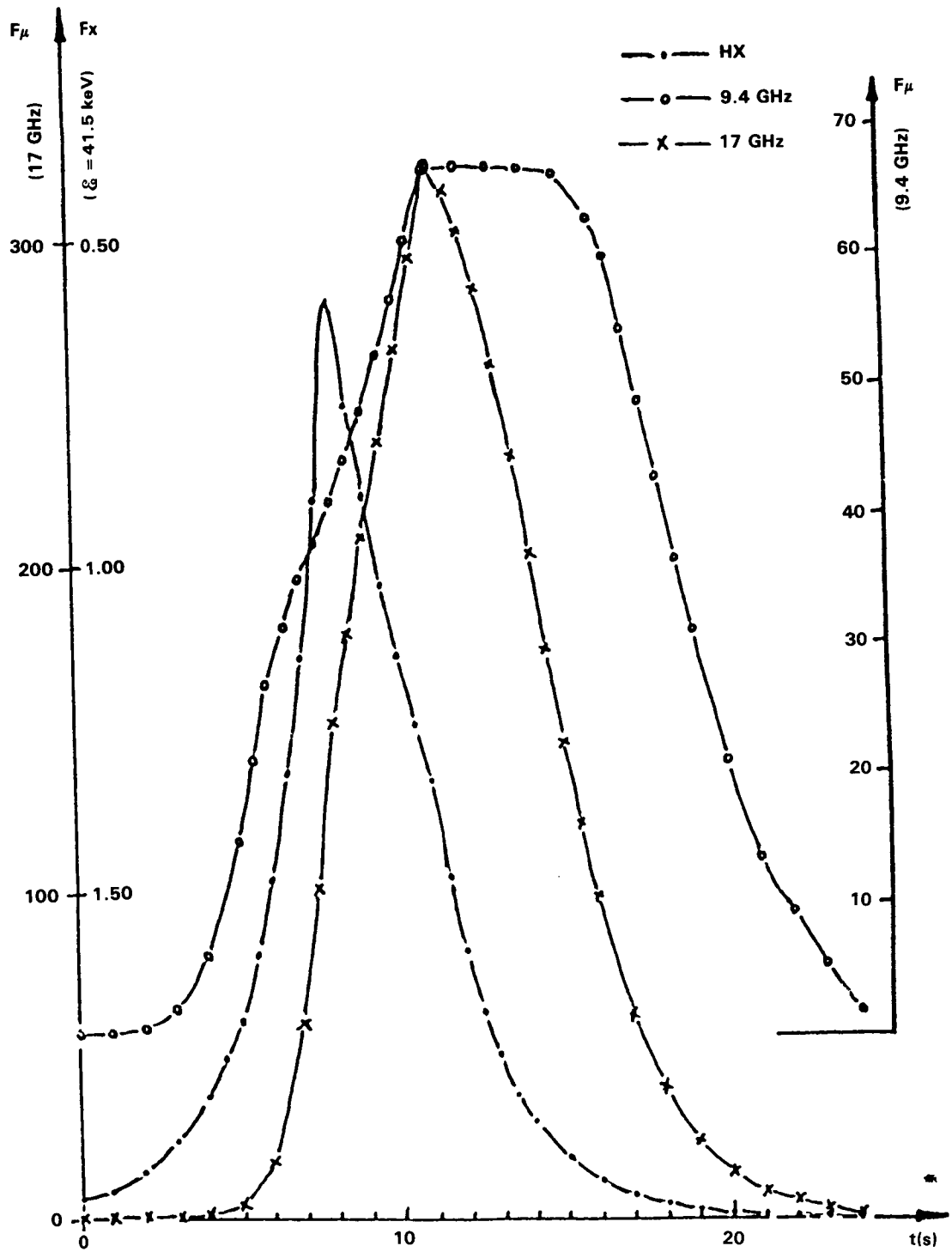


Figure 5b. The same as Figure 5a, but corresponding to case (b) in Figure 4, with an unsymmetric time profile for $N(t)$.

V. Conclusions and Discussions

Starting with the systematic analysis of the spectra of the impulsive MW and HX bursts, we investigated the correlation of the spectral indices and found a possible way to distinguish between the thermal and nonthermal models. Comparisons of the theoretical results with the observations show that only the nonthermal models can explain the optically-thin MW spectrum and its relation to the HX spectrum. The results suggest that both the impulsive HX and MW bursts are produced by the same population of nonthermal electrons accelerated during the impulsive phase. The relative time delays of HX and MW can be explained consistently in a magnetic trap model if only the hardening of the electron spectrum is considered.

All the discussions above are simplified and the results are preliminary. We should have more data to plot the δ - γ correlation diagram and construct the model in more detail. In Figure 2 the δ - γ correlation is for different events. It would be obviously of great significance to analyse the δ - γ correlation during the lifetime of one event (or during its impulsive phase). But it is not easy to get the simultaneous HX and high-frequency MW spectral data.

References

- Bai, T. et al. 1983, Ap.J., 267, 433
Benz, A.O. 1977, Ap.J., 211, 270
Brown, J.C. 1974 in Coronal Disturbances, Newkirk ed., IAU Symposium, No. 53, 395
Brown, J.C. 1976, Phil. Trans. R. Soc. Lond. A., 281, 473
Crannell, C.J. et al. 1978, Ap.J., 223, 620
Das, T.K. and Das Gupta, M.K. 1983, Bull. Astron. Inst., Czechoslovakia, 34, 229
Dulk, G.A. and Dennis, B.R. 1982, Ap.J., 260, 875
Dulk, B.A. et al. 1979, Ap.J., 234, 1137
Emsile, A.G. 1983, Solar Phys., 86, 133
Enome, S. 1982 in Hinotori Symposium on Solar Flares 1982, p. 263
Guidice, D.A. and Castelli, J.P. 1975, Solar Phys., 44, 155
Hoyng, P. et al. 1976, Solar Phys., 48, 197
Kane, S.R. et al. 1983, Ap.J., 271, 376
Kaufmann, P. et al. 1983, Solar Phys., 84, 311
Matzler, C. 1978, A.Ap., 70, 181
Takakura, T. et al. 1984, Solar Phys., 89, 379
Tandberg-Hansen, E. et al. 1984, Solar Phys., 90, 41
Wiehl, H. et al. 1980, A. Ap., 92, 260.